BJR

https://doi.org/10.1259/bjr.20180756

Received: 30 August 2018 | Revised: 18 October 2018 | Accepted: 03 January 2019

Cite this article as:
Reinert CP, la Fougère C, Nikolaou K, Pfannenberg C, Gatidis S. Value of CT iterative metal artifact reduction in PET/CT—clinical evaluation in 100 patients. *Br J Radiol* 2019; **92**: 20180756.

FULL PAPER

Value of CT iterative metal artifact reduction in PET/CT—clinical evaluation in 100 patients

[1]CHRISTIAN PHILIPP REINERT, MD, [2]CHRISTIAN LA FOUGÈRE, MD, [1]KONSTANTIN NIKOLAOU, MD, [1]CHRISTINA PFANNENBERG, MD and [1]SERGIOS GATIDIS, MD

[1]Department of Diagnostic and Interventional Radiology, University Hospital Tuebingen, Tuebingen, Germany
[2]Department of Nuclear Medicine and Clinical Molecular Imaging, University Hospital Tuebingen, Tuebingen, Germany

Address correspondence to: Dr Christian Philipp Reinert
E-mail: *christian.reinert@med.uni-tuebingen.de*

Objective: To assess the technical feasibility and diagnostic benefit of CT iterative metal artifact reduction (iMAR) in patients with metal implants undergoing positron emission tomography (PET/CT.

Methods: PET/CTs of 100 patients with metal implants in different anatomical localization were retrospectively analyzed. CT data were reconstructed with iMAR and without iMAR (noMAR) and used in comparison for PET attenuation correction, generating iMAR-corrected and noMAR PET data. The effect of iMAR on quantitative CT and PET analysis was assessed by measurements of Hounsfield units (HUs) and standard uptake values (SUV) in predefined anatomical structures and pathological lesions in the vicinity of metal implants. Diagnostic confidence for lesion delineation was assessed using a 3-point scale.

Results: For artifact-affected structures, mean HU of iMAR corrected CT significantly differed compared to noMAR CT and standard deviations were significantly lower [*e.g.* M. masseter: 71.01 ± 22.34 HU (iMAR) *vs* 98.89 ± 92.18 HU (noMAR), $p < .01$]. SUVs did not significantly differ in artifact-affected structures [*e.g.* M. masseter: SUVmean 0.96 ± 0.54 (iMAR) *vs* 0.97 ± 0.55 (noMAR); $p > .89$] and pathological findings [SUVmean 10.78 (iMAR) *vs* 10.81 (noMAR); $p > .98$] between iMAR and noMAR PET. Qualitatively, delineation was significantly improved in iMAR corrected CT for the interpretation of anatomical and pathological structures [*e.g.* score of pathologic lesions: 2.80 (iMAR) *vs* 2.31 (noMAR); $p < .01$].

Conclusion: The use of iMAR in PET/CT significantly improves delineation of anatomical and pathological structures in the vicinity of metal implants in CT. PET quantification and PET image quality are not significantly affected by the use of iMAR-based attenuation correction independent of the presence of metal implants.

Advances in knowledge: IMAR is a feasible algorithm in PET/CT improving CT image quality in the vicinity of metal implants without affecting PET quantification and can therefore be implemented in the clinical routine.

INTRODUCTION

Position emission tomography (PET)/CT is widely used for diagnosis, response monitoring and radiotherapy planning in a variety of oncologic, neurologic and inflammatory disorders. Its high diagnostic accuracy in localization and characterization of diverse pathological processes derives from the combination of high-resolution CT and molecular imaging provided by PET within a single examination allowing for a precise spatial allocation of tracer uptake.[1] Moreover, the combination of PET and CT allows for efficient CT based attenuation correction of PET images.

Metal implant-related artifacts are quite common in CT images, for instance, in patients with high-density objects such as dental fillings, orthopedic hardware, and surgical clips or coils, resulting in corrupted projection data that generate bright and dark streaking artifacts in the reconstructed CT image.[2] Artifacts caused by metallic implants lead to impaired image quality of the adjacent tissue and the metallic implant itself. Thus, the measured tissue attenuation values (*i.e.* CT Hounsfield units, HUs) can be highly inaccurate around high-density objects. Artifacts which obscure relevant anatomic structures increase the risk of missing pathological findings. The degree of X-ray attenuation and physical effects differ depending on the size and composition of the metallic implant.[3] CT-based PET attenuation correction is susceptible to errors in regions where CT artifacts occur, particularly in the vicinity of metal implants, and can cause falsely low or high measured local tracer activity concentrations.[4,5] To reduce CT metal artifacts several approaches have been introduced. Artifacts that are due to photon starvation are primarily suppressed

by the projection-based metal artifact reduction (MAR) algorithm. This dual-energy CT-based technique suppresses the effects of beam hardening by extrapolation of high photon energy scans and by computation of monoenergetic CT images.[6,7] In addition, post-processing CT reconstruction techniques allow for a reduction in CT metal artifacts. As attenuation correction of PET images depends on CT data, MARs have been proven advantageous for reduction of metal artifacts in PET/CT.[8–10] An iterative MAR (iMAR) algorithm as a combination of normalized and frequency-split MAR has been proven particularly efficient in the reduction of CT metal artifacts.[11–13] In two recently performed phantom studies, it markedly improved image quality and PET quantification[14] and was superior compared to dual-energy-based MAR strategies in reducing CT metal artifacts and PET quantification errors.[15]

The purpose of this retrospective study was to test the hypothesis that the use of dedicated CT(CT) iMAR algorithms can significantly improve diagnostic confidence in patients with various metal implants undergoing PET/CT with different F-18 as well as Ga-68 labelled radiotracers.

METHODS AND MATERIALS

Study population

This retrospective study was approved by the local institutional ethical review board and informed consent was waived (Project Number: 294/2018BO).

The underlying study population consisted of patients undergoing clinically indicated at the PET/CT center of the Tuebingen University Hospital between October 2017 and March 2018. From this population, all patients with intracorporal metal implants and who presented with a clinical question referring to the anatomical region of the metal implants (suspected or present local malignancy) were included in the study.

PET/CT imaging

All PET/CT examinations were performed on a state-of-the art clinical scanner (Biograph mCT, Siemens Healthineers, Knoxville, TN). Approximately 300 MBq [^{18}F] fludeoxyglucose (FDG), 185 MBq [^{68}Ga] PSMA-HBED-CC or 185 MBq [^{68}Ga]-DOMITATE were injected intravenously 60 min prior to image acquisition. To reduce beam-hardening artifacts and motion artifacts all patients were positioned in the scanner with raised arms and in a vacuum mattress. We used standardized CT examinational protocols. Portal-venous phase acquisitions were obtained with 70 s delay time using a tube voltage of 120 kV and a reference dose of 200 mAs. Depending on the clinical indication, CT examinations were performed with weight-adapted 90–120 ml intravenous CT contrast agent (Ultravist 370; Schering AG, Berlin, Germany), which was given intravenously at a rate of 2 ml s^{-1} followed by a 30 ml saline chaser, or without a contrast agent. Dedicated head and neck examination protocols were used in patients with cervical cancer and metastases. These patients had to place their arms sideways to the body trunk for the head/neck scan. All included PET/CT examinations were acquired in full-dose technique. Image reconstruction was performed in all patients using iterative CT reconstruction (Siemens SAFIRE, Forchheim, Germany; with and without iMAR), with a soft tissue kernel, an axial slice thickness of 3 mm and an increment of 2 mm. The mean CTDIvol was 25.9 ± 7.7 mGy and the mean dose–length product was 1607.4 ± 299.8 mGycm.

PET was acquired from the skull base to the mid-thigh level over six to eight beds and reconstructed using a three-dimensional ordered subset expectation maximization algorithm (2 iterations, 21 subsets, Gaussian filter 2.0 mm, matrix size 400 × 400, and slice thickness 2.0 mm). The PET acquisition time was 2 min per Bed position. PET data were reconstructed once using noMAR CT and once using iMAR CT for the purpose of attenuation correction. In our study the same iMAR algorithm was used for all included PET/CT examinations. This iMAR algorithm was provided by Siemens Healthcare (Erlangen, Germany). All reconstructions were performed on the scanner.

Image analysis

Image analysis of iMAR corrected and noMAR CT and PET images was performed both quantitatively and qualitatively.

For quantitative analysis, circular regions of interests (ROIs) were manually placed in previously defined anatomic structures in the vicinity of metallic hardware on noMAR CT images, including parts of both bright and dark streak artifacts. In case of metallic hardware in the head and neck region (dental fillings or implants), we placed ROIs in the Septum linguae and the M. masseter which are anatomical regions most affected by streak artifacts, and also in the M. sternocleidomastoideus which is often localized in a border area of streak artifacts. In case of orthopedic hardware in the pelvic region (endoprostheses of the hip, surgical clips/coils), we placed ROIs in the M. iliopsoas, M. gluteus maximus and bladder, respectively. In case of other metal implants (pace maker, internal fixator), ROIs were placed in in a similar way. To examine effects of iMAR on CT-HU and PET-standard uptake value (SUV) measurements of not artifact-affected anatomical structures we placed ROIs within the liver parenchyma and the right atrium.

The size of the ROIs was chosen as large as possible in the anatomical structures of interest (carefully excluding neighboring anatomical structures). However, to ensure valid and robust measurements, we did not fall below a minimal ROI diameter of 10 mm.

ROIs were subsequently copied to the respective position of the iMAR CT and the noMAR and iMAR PET data sets.

For each CT ROI, mean attenuation numbers (HUs) with standard deviation (SD) were recorded. For each PET ROI, SUVmean as well as SUVmax were recorded.

In order to evaluate the effect of iMAR on pathological findings, we selected a maximum of two visible pathologic lesions in the vicinity of metallic hardware. We measured the maximum diameter in CT and the SUVmean of these lesions in iMAR PET and noMAR PET. For each lesion we documented if it was completely overlayed by streak artifacts derived from metallic hardware,

not overlayed or if it was localized in the border area of streak artifacts.

For qualitative analysis, all image data were assessed by two radiologists in consensus. First, the magnitude of metal artifacts in CT and PET was evaluated on a 3-point Likert scale (1, strong artifacts; 2, moderate artifacts; 3, weak artifacts). Furthermore, the delineation of pathologic lesions in CT and PET was assessed using a 3-point Likert scale (1, poorly delineated; 2, fairly delineated; 3, well delineated). Images which were rated score 1 ("poorly delineated") were non-diagnostic due to total overlaid of the relevant structure by bright and/or dark streak artifacts. In images which were scored 2 ("fairly delineated"), the delineation of relevant structures was significantly reduced by bright and/or dark streak artifacts, however, a limited interpretability regarding the relevant structure remained. In images which were scored 3 ("well delineated") relevant structures were almost completely delineated with at most little impairment of bright and/or dark streak artifacts.

Statistics

All statistical calculations and graphical illustrations were performed using SPSS v.n 22 (IBM Corporation, Armonk, North Castle, NY). First, we used the Kolmogorov–Smirnov test for testing the Gaussian distribution of the variables. Second, to statistically analyze quantitative differences of the dependent variables across the iMAR corrected and noMAR CT and PET images, a test for homogeneity of variances (Levene's test) was performed. To statistically analyze differences of image quality using a 3-point-Likert scale, we performed a Mann–Whitney *U* test. The significance level was set at a *p*-value of < .05.

RESULTS

Study population

100 consecutive patients [30 female; mean age 67 (35-90) years; body mass index (BMI) 24.4 ± 3.8 kg/m^2] were included. The distribution of metal implants was as follows: dental fillings or implants containing components of silver, copper, tin and mercury (78/100), orthopedic hip endoprostheses which were either composed of chrome-molybdenum-alloys (in case of cemented prostheses) or titanium alloys (bone-ingrown prostheses) (16/100), and other, titanium containing metallic hardware (6/100) including a cardiac pacemaker (1/6), internal fixators of the spine (2/6), surgical coils in the right lower abdomen (1/6) and a screw fixation in the femoral neck (1/6). 38/78 patients with dental fillings or implants had a primary head and neck tumor while 40/78 had secondary metastases in the head and neck region. 12/16 patients with orthopedic hardware in the hip region had primary pelvic malignancies, 4/16 secondary metastases, respectively.

The following PET tracers were used, [^{18}F]-FDG in 75 patients and ^{68}Ga-PSMA-HBED-CC in 25 patients. Due to the small number of patients with metal implants presenting with a suspected or present local malignancy who underwent ^{68}Ga-DOMITATE-PET/CT examination (N = 3) we excluded these patients in our analysis.

Effect of iMAR on CT HU in anatomical structures

In 82/100 patients, a total number of 122 pathologic lesions in the vicinity of metallic hardware were identified, 42/82 patients had one lesion, 40/82 patients had two lesions, respectively. 46 lesions were localized in the close proximity of streak artifacts, 58/122 lesions were outside of the field of streak artifacts and 18/122 lesions were localized in a border area.

In iMAR corrected CT images of patients with dental fillings or implants the mean HU of the most artifact affected anatomical structures were significantly lower than in noMAR CT [M.masseter: 71.01 ± 22.34 HU (iMAR) *vs* 98.89 ± 92.18 HU (noMAR), $p < .01$; Septum linguae: 88.41 ± 35.11 HU (iMAR) *vs* 118.88 ± 217.76 HU (noMAR), $p < .01$]. The mean HU values of the M. sternocleidomastoideus located in the border area of artifacts were significantly higher [56.75 ± 20.12 HU (iMAR) *vs* 48.05 ± 35.21 HU (noMAR), $p < .01$] (Figure 1a). The mean voxelwise ROI standard deviations of HU were significantly higher in the noMAR CT images for all measured physiological anatomical structures, respectively ($p < .01$) (Figure 1b).

Similarly, in iMAR corrected CT images of patients with orthopedic hip endoprostheses the mean HU of the most artifact affected anatomical structures were significantly lower than in the noMAR CT images [M. gluteus maximus: 49.13 ± 21.32 HU (iMAR) *vs* 79.51 ± 62.18 HU (noMAR), $p < .05$; M. iliopsoas: 48.08 ± 24.96 HU (iMAR) *vs* 113.94 HU ± 66.59 HU (noMAR), $p < .01$], except of the bladder where the mean HU were significantly higher [−0.22 ± 20.57 HU (iMAR) *vs* −79.65 ± 126.96 HU (noMAR), $p < .01$] (Figure 2a). The respective mean voxelwise ROI standard deviations of HU were significantly lower in the M. iliopsoas ($p < .05$) and in the bladder ($p < .01$), while the mean standard deviations of the M. gluteus maximus located in the border area of artifacts did not differ significantly between the iMAR-corrected and noMAR CT images (Figure 2b)..

Also, in the third cohort of subjects with other metallic hardware the mean HU values of the neighboring anatomical structures were significantly lower in the iMAR corrected CT images than in the noMAR CT images [65.55 ± 30.21 HU (iMAR) *vs* 102.26 ± 86.31 HU (noMAR), $p < .05$] (Figure 3). The standard deviations were significantly higher in the noMAR CT images, respectively ($p < .01$) (Figure 3).

The use of iMAR did not affect CT HU of not artifact-affected anatomical structures: Mean HU liver: 98.62 ± 21.22 HU [iMAR] *vs* 98.48 ± 21.10 HU [noMAR], $p > .95$; SD liver: 25.71 ± 39.39 [iMAR] *vs* 24.19 ± 38.35 HU [noMAR], $p > .87$; mean HU right atrium: 163.02 ± 39.63 HU [iMAR] *vs* 163.04 ± 39.63 HU [noMAR], $p > .99$; SD right atrium: 29.58 ± 56.71 HU [iMAR] *vs* 28.79 ± 56.32 HU [noMAR], $p > .97$.

Effect of iMAR on PET SUV in anatomical structures

Regarding the quantification of the PET SUV in iMAR corrected and noMAR PET images the measured SUVmean/max of the defined ROIs within anatomical structures in the area of present metal implants did not show significant differences. In

Figure 1. Effect of iMAR on mean HU ± 95% CI of the most artifact-affected anatomical structures M. masseter and Septum linguae in the vicinity of dental fillings/implants and on mean HU of the M. sternocleidomastoideus located in the border area of artifacts. iMAR corrected CT HU marked with two asterisks differ significantly from noMAR CT HU ($p < .01$). (b) Effect of iMAR on mean voxelwise HU standard deviation ± 95% CI of the most artifact-affected anatomical structures M. masseter and Septum linguae in the vicinity of dental fillings/implants and on mean HU of the M. sternocleidomastoideus located in the border area of artifacts. iMAR corrected CT HU marked with two asterisks differ significantly from noMAR CT HU ($p<.01$). CI, confidence interval; HU, Hounsfield unit; iMAR, iterative metal artifact reduction.

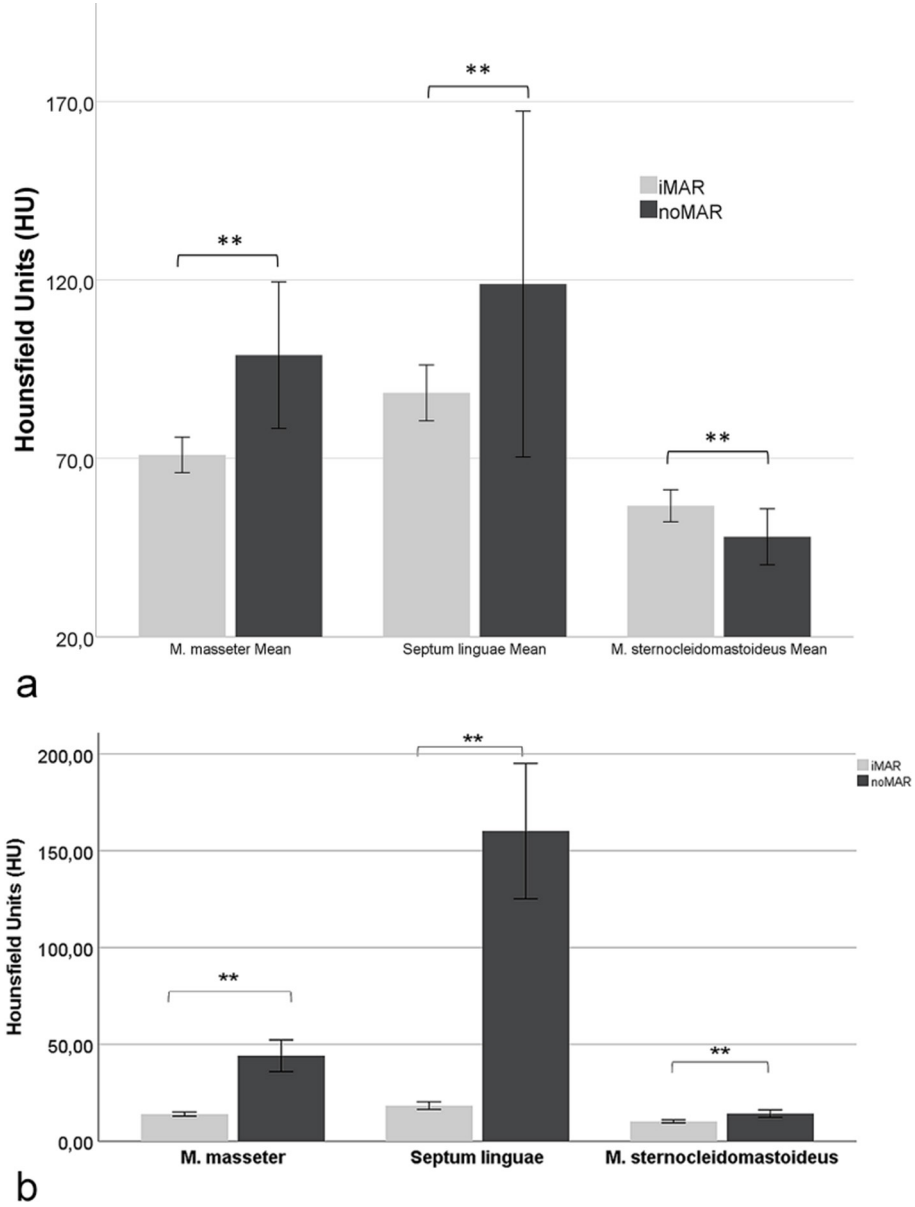

addition, the use of iMAR did not affect PET SUV measurements in not artifact-affected anatomical structures ($p > .99$) (Figure 4).

Effect of iMAR on lesion PET quantification and lesion delineation in CT

The mean size of the detected pathologic lesions near metallic hardware in the head and neck region was 1.50 cm (range, 0.6–4.15 cm), and in the hip region it was 1.58 cm (range, 0.66–2.54 cm). In the third cohort of subjects with other metallic hardware the mean size of the detected pathologic lesions was 3.27 cm (range, 1.28–6.31 cm). Comparing the SUVmean/max of all pathologic lesions in iMAR corrected and noMAR corrected PET images irrespectively of the anatomical region, the values did not show significant differences [SUVmean: 10.78 ± 10.49 (iMAR) *vs* 10.81 ± 10.50 (noMAR), $p > .98$; SUVmax 16.27 ± 16.33 (iMAR) *vs* 16.31 ± 16.28 (noMAR), $p > .99$] (Figure 4). The two different tracers and radionuclides used for the examinations, [^{18}F]-FDG and [^{68}Ga]-PSMA-HBED-CC, did not impact the measured SUVmean of

Figure 2. Effect of iMAR on mean HU ± 95% CI of the most artifact-affected anatomical structures M. gluteus maximus, M. iliopsoas and bladder in the vicinity of hip endoprostheses. iMAR corrected CT HU marked with asterisks differ significantly from noMAR CT HU (*= $p < .05$; **=$p < .01$) (b) Effect of iMAR on mean voxelwise HU standard deviation ± 95% CI of the most artifact-affected anatomical structures M. gluteus maximus, M. iliopsoas and bladder in the vicinity of hip endoprostheses. iMAR corrected CT HU marked with asterisks differ significantly from noMAR CT HU (* = $p < .05$; **=$p < .01$). CI, confidence interval; HU, Hounsfield unit; iMAR, iterative metal artifact reduction.

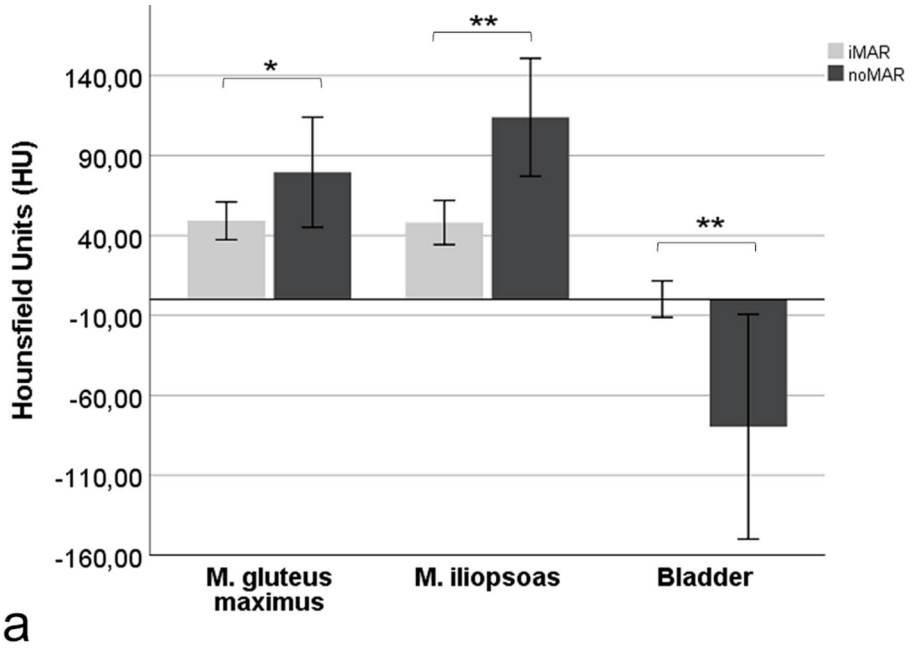

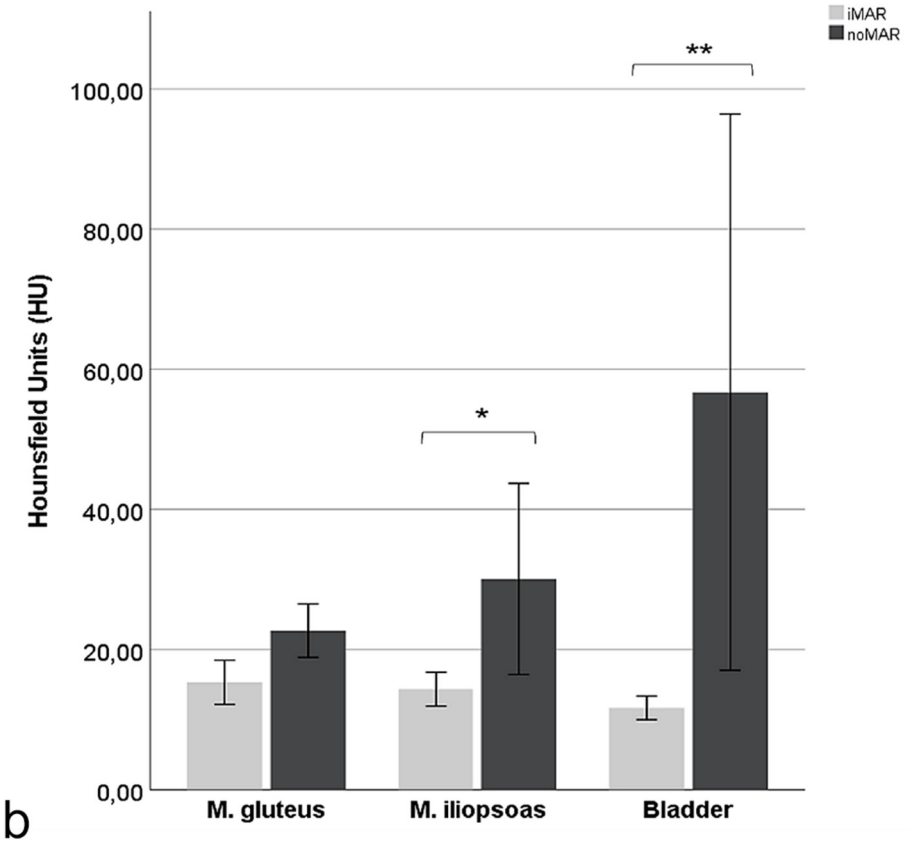

Figure 3. Effect of iMAR on mean HU ± 95% CI (left) and on mean voxelwise HU standard deviation ±95% (right) of three most artifact-affected anatomical structures in the vicinity of other metal implants (cardiac pacemaker, internal fixators of the spine, surgical clips/coils, screw fixation in the femoral neck). iMAR corrected CT HU marked with asterisks differ significantly from noMAR CT HU (*= $p < .05$; **=$p < .01$). CI, confidence interval; HU, Hounsfield unit; iMAR, iterative metal artifact reduction.

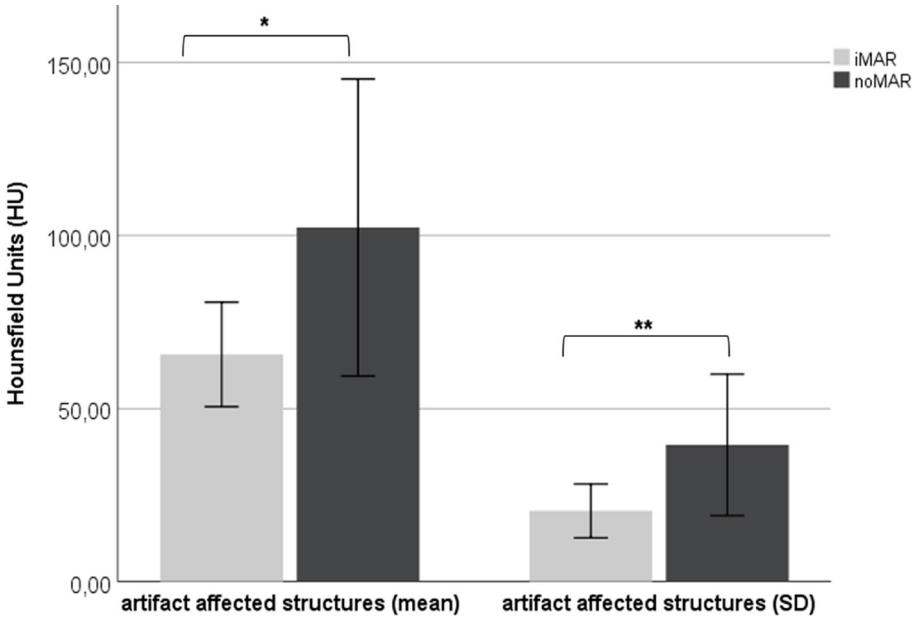

normal anatomical structures in iMAR and noMAR corrected PET images in the case of dental implants/fillings (Figure 5a) and hip endoprostheses (Figure 5b).

The assessment of the subjective image quality using a 3-point scale by two independent radiologists showed significant differences comparing the severity of artifacts in iMAR corrected and noMAR CT images for the analysis of the above-mentioned physiological anatomical structures ($p < .01$) (Figure 6). Also, the delineation of pathologic lesions in CT was significantly improved by iMAR ($p < .01$)(Figure 6). No significant difference in visual image information was observed between iMAR and

Figure 4. Effect of iMAR on SUVmean/max ± 95% CI of pathologic lesions (n = 122) in the vicinity of all included metal implants and effect of iMAR on the not artifact affected liver and blood pool, showing no significant differences between iMAR corrected PET SUV and noMAR PET SUV. CI, confidence interval, HU, Hounsfield unit; iMAR, iterative metal artifactreduction; SUV, standard uptake value.

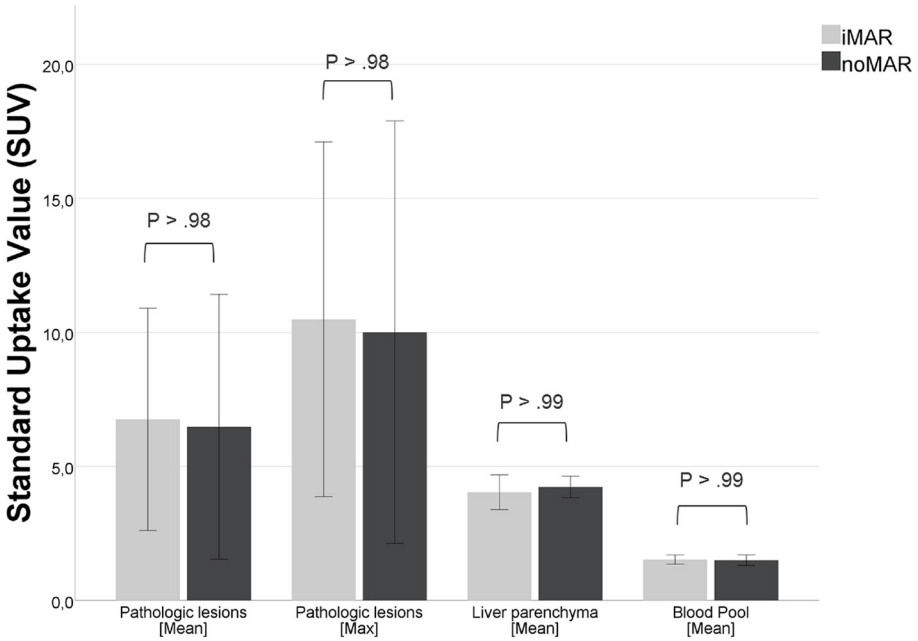

Figure 5. Effect of iMAR on SUVmean ± 95% CI of anatomical structures in the vicinity of dental implants/fillings comparing the use of [^{18}F]-FDG and [^{68}G]-PSMA Abbreviation: M. sternocleidomastoideus (M. SCM). (b) Effect of iMAR on SUVmean ± 95% CI of anatomical structures in the vicinity of hip endoprostheses comparing the use of [^{18}F]-FDG and [^{68}G]-PSMA. CI, confidence interval; FDG, fludeoxyglucose; HU, Hounsfield unit; iMAR, iterative metal artifact reduction; SUV, standard uptake value.

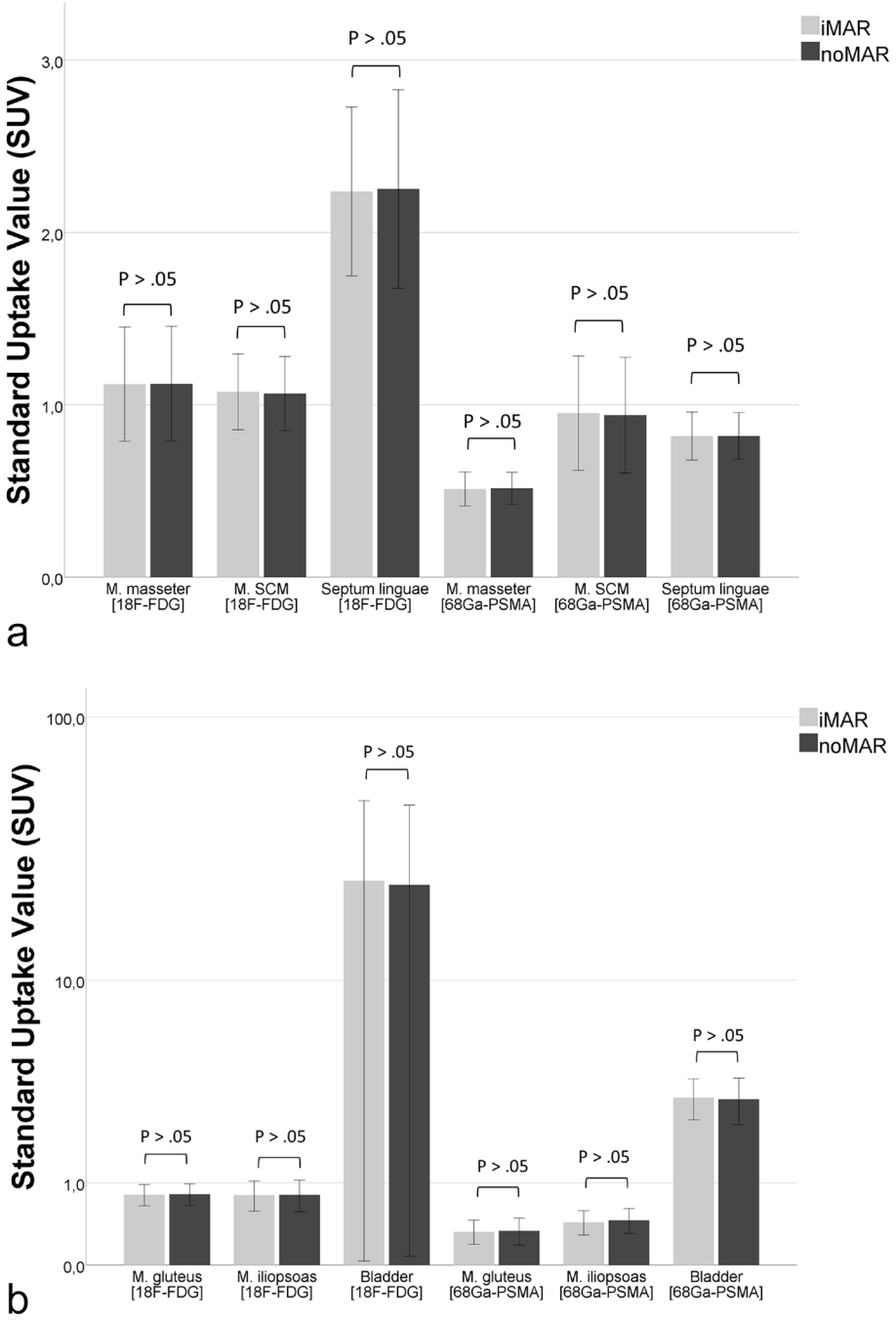

noMAR corrected PET concerning the delineation of tracer-avid pathologic lesions (Figure 7).

DISCUSSION

In this study we systematically investigated the quantitative and qualitative effect of iterative metal artifact reduction on PET/CT with respect to quantification of CT HU and PET SUV as well as delineation of pathologic lesions.

We observed a significant improvement of CT image quality and lesion delineation using iMAR and a significant effect of iMAR on quantification of CT HU. However, no relevant impact of iMAR-based attenuation correction on PET quantification and PET image quality could be observed. Furthermore, the use of iMAR did not affect CT HU or PET SUVs in anatomic regions that were not affected by metal artifacts.

Figure 6. 3-point Likert scale showing the effect of iMAR on the subjective image quality rated by two independent radiologists. Severity of artifacts in iMAR corrected and noMAR CT for the analysis of anatomical structures (left side; score ±95% CI) and delineation of pathologic lesions in iMAR corrected and noMAR CT (right side; score ±95% CI). Scores of iMAR corrected CT marked with two asterisks differ significantly from noMAR CT ($p < .01$). CI, confidence interval; HU, Hounsfield unit; iMAR, iterative metal artifact reduction; SUV, standard uptake value.

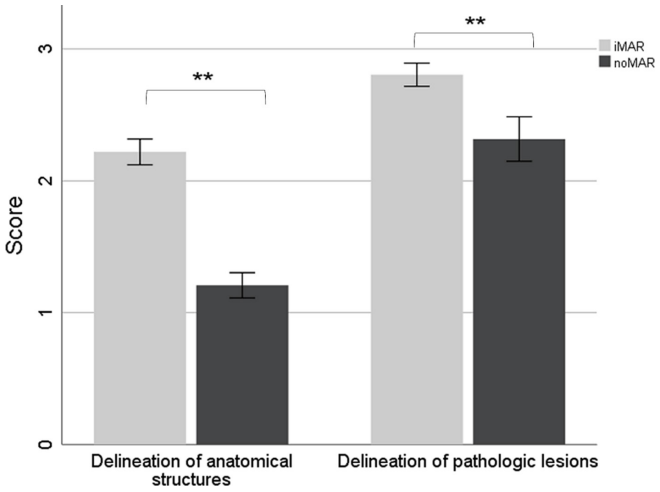

Figure 7. Impact of iMAR on delineation of a retroperitoneal lymph node metastasis in the vicinity of an internal fixator [A, score 1 (noMAR) *vs* score 2 (iMAR)], a sigmoid carcinoma adjacent to coils in the right A. iliaca interna [B, score 1 (noMAR) *vs* score 2 (iMAR)] and a lymph node metastasis in neck level III in the vicinity to dental implants [C, score 1 (noMAR) *vs* score 2 (iMAR)]. The respective lesions are poorly delineable in noMAR CT (upper rows, left columns) while iMAR improves its delineation (upper rows, right columns). No impact of iMAR on PET quantification and qualitative PET evaluation was observed [bottom rows, *e.g.* dental implants, SUVmean 16.9 (iMAR) *vs* 16.8 (noMAR)]. CI, confidence interval; HU, Hounsfield unit; iMAR, iterative metal artifactreduction; SUV, standard uptake value.

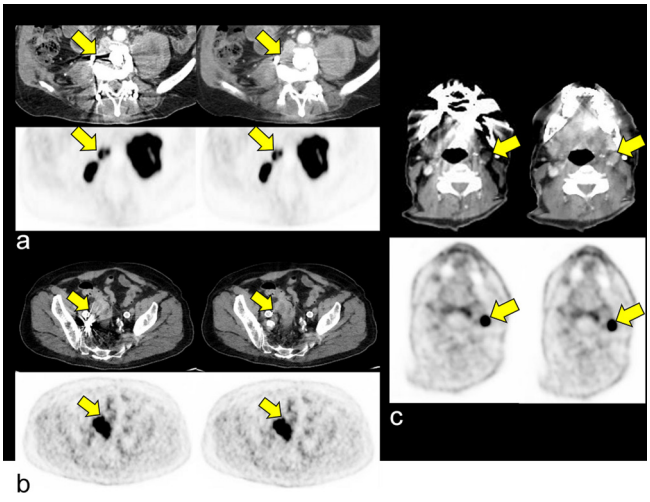

These results are in good concordance with previous studies showing that the use of iMAR can improve CT image quality in the vicinity of metal implants.[11,12,15,16] Weiss et al demonstrated the potential of iMAR in reducing streak artifacts and thus improving visualization of anatomic structures.[17] iMAR has been shown to allow for more effective reduction of metal artifacts compared to a dual energy based methods.[18]

In contrast to our study, previous studies on MAR algorithms in PET/CT demonstrated an under- and overestimation of [^{18}F]-FDG activity concentration in the most artifact-affected areas around metal prostheses as a result of dark and bright streak artifacts.[4,8,19] For example, an improvement of image quality and PET quantification using iMAR-based attenuation correction was observed in recently performed phantom studies. Harnish et al demonstrated that iMAR-based attenuation correction results in more accurate PET quantification using an experimental phantom design.[20] In another phantom study performed by Schabel et al a reduction of both, metal streak artifacts and PET quantification errors around the dental implants was observed using iMAR compared to the data sets without iMAR.[14]

However, in these previous studies, PET measurements were performed directly in regions of the strongest presence of bright or dark streak artifacts leading to higher overestimation or underestimation of HU in CT with consecutive relevant PET quantification errors. In a similar way, Van der Vos et al analyzed attenuation corrected PET data by standard CT and iMAR-processed CT of 21 patients with metal implants both quantitatively and qualitatively.[21] They also observed an underestimation of SUVmean values in areas with underestimated HU located directly in dark streak artifacts and an overestimation of SUVmean values in areas located directly in bright streaks artifacts, respectively. However, these observed differences in tracer uptake quantification were only minimal. Furthermore, in this previous study, attenuation correction was performed using low-dose CT scans which may result in an increased susceptibility to metal artifacts.

In contrast to these previous studies, we analyzed a large number of patients with different metallic implants in a clinical setting. We guided the ROI placement by anatomical structures and by pathological lesions involving both bright and dark streaks artifacts of variable degree in order to ensure that our measurements mirror the diagnostic demands of the daily routine rather than placing ROIs directly within the region of strongest artifacts. Using this setting, no significant quantitative or qualitative impact of iMAR-based attenuation correction on PET was observed in our study.

Our study has limitations. Due to the retrospective study design it is not possible to value the use of iMAR for diagnostic decisions and implications for patient outcomes. Further prospective studies are necessary to investigate whether iMAR is a tool that directly influences diagnostic decisions by improving both sensitivity and specificity and thus may be advantageous for patient outcome. However, to our knowledge, this is the first study that evaluates the clinical use of iMAR in a large patient collective with different metallic hardware demonstrating the clinical potential of iMAR.

CONCLUSIONS

In conclusion, iMAR is a useful algorithm to significantly improve delineation of both anatomical and pathological structures in the vicinity of metal implants in CT. Furthermore, in a clinical diagnostic setting, no significant influence of iMAR-based attenuation correction on PET quantification and PET image quality could be observed independently of the presence of metal implants.

REFERENCES

1. von Schulthess GK, Steinert HC, Hany TF. Integrated PET/CT: current applications and future directions. *Radiology* 2006; **238**: 405–22. doi: https://doi.org/10.1148/radiol.2382041977
2. Robertson DD, Yuan J, Wang G, Vannier MW. Total hip prosthesis metal-artifact suppression using iterative deblurring reconstruction. *J Comput Assist Tomogr* 1997; **21**: 293–8. doi: https://doi.org/10.1097/00004728-199703000-00024
3. Yadava GKP, Pal D, Hsieh J. Reduction of metal artifacts: beam hardening and photon starvation effects. *Proceedings of the SPIE* 2014; **9033**(id 90332V 8 pp).
4. Goerres GW, Ziegler SI, Burger C, Berthold T, Von Schulthess GK, Buck A. Artifacts at PET and PET/CT caused by metallic hip prosthetic material. *Radiology* 2003; **226**: 577–84. doi: https://doi.org/10.1148/radiol.2262012141
5. Purohit BS, Ailianou A, Dulguerov N, Becker CD, Ratib O, Becker M. FDG-PET/CT pitfalls in oncological head and neck imaging. *Insights Imaging* 2014; **5**: 585–602. doi: https://doi.org/10.1007/s13244-014-0349-x
6. Zhang Y, Zhang L, Zhu XR, Lee AK, Chambers M, Dong L. Reducing metal artifacts in cone-beam CT images by preprocessing projection data. *Int J Rad Oncol *Biol* Phys* 2007; **67**: 924–32. doi: https://doi.org/10.1016/j.ijrobp.2006.09.045
7. Pessis E, Campagna R, Sverzut JM, Bach F, Rodallec M, Guerini H, et al. Virtual monochromatic spectral imaging with fast kilovoltage switching: reduction of metal artifacts at CT. *Radiographics* 2013; **33**: 573–83. doi: https://doi.org/10.1148/rg.332125124
8. Abdoli M, Dierckx RA, Zaidi H. Metal artifact reduction strategies for improved attenuation correction in hybrid PET/CT imaging. *Med Phys* 2012; **39**(6Part1): 3343–60. doi: https://doi.org/10.1118/1.4709599
9. Lell MM, Meyer E, Kuefner MA, May MS, Raupach R, Uder M, et al. Normalized metal artifact reduction in head and neck computed tomography. *Invest Radiol* 2012; **47**: 415–21. doi: https://doi.org/10.1097/RLI.0b013e3182532f17
10. Schäfers KP, Raupach R, Beyer T. Combined 18F-FDG-PET/CT imaging of the head and neck. An approach to metal artifact correction. *Nuklearmedizin* 2006; **45**: 219–22.
11. Morsbach F, Bickelhaupt S, Wanner GA, Krauss A, Schmidt B, Alkadhi H. Reduction of metal artifacts from hip prostheses on CT images of the pelvis: value of iterative reconstructions. *Radiology* 2013; **268**: 237–44. doi: https://doi.org/10.1148/radiol.13122089
12. Meyer E, Raupach R, Lell M, Schmidt B, Kachelrieß M. Frequency split metal artifact reduction (FSMAR) in computed tomography. *Med Phys* 2012; **39**: 1904–16. doi: https://doi.org/10.1118/1.3691902
13. Meyer E, Raupach R, Lell M, Schmidt B, Kachelriess M. Normalized metal artifact reduction (NMAR) in computed tomography. *Med Phys* 2010; **37**: 5482–93. doi: https://doi.org/10.1118/1.3484090
14. Schabel C, Gatidis S, Bongers M, Hüttig F, Bier G, Kupferschlaeger J, et al. Improving CT-based PET attenuation correction in the vicinity of metal implants by an iterative metal artifact reduction Algorithm of CT data and its comparison to Dual-Energy-Based strategies: a phantom study. *Invest Radiol* 2017; **52**: 61–5. doi: https://doi.org/10.1097/RLI.0000000000000306
15. Morsbach F, Wurnig M, Kunz DM, Krauss A, Schmidt B, Kollias SS, et al. Metal artefact reduction from dental hardware in carotid CT angiography using iterative reconstructions. *Eur Radiol* 2013; **23**: 2687–94. doi: https://doi.org/10.1007/s00330-013-2885-z
16. Higashigaito K, Angst F, Runge VM, Alkadhi H, Donati OF. Metal artifact reduction in pelvic computed tomography with hip prostheses: comparison of virtual Monoenergetic Extrapolations from dual-energy computed tomography and an iterative metal artifact reduction algorithm in a phantom study. *Invest Radiol* 2015; **50**: 828–34. doi: https://doi.org/10.1097/RLI.0000000000000191
17. Weiß J, Schabel C, Bongers M, Raupach R, Clasen S, Notohamiprodjo M, et al. Impact of iterative metal artifact reduction on diagnostic image quality in patients with dental hardware. *Acta Radiol* 2017; **58**: 279–85. doi: https://doi.org/10.1177/0284185116646144
18. Bongers MN, Schabel C, Thomas C, Raupach R, Notohamiprodjo M, Nikolaou K, et al. Comparison and combination of Dual-Energy- and Iterative-Based metal artefact reduction on hip prosthesis and dental implants. *PLoS One* 2015; **10**: e0143584. doi: https://doi.org/10.1371/journal.pone.0143584
19. Kamel EM, Burger C, Buck A, von Schulthess GK, Goerres GW. Impact of metallic dental implants on CT-based attenuation correction in a combined PET/CT scanner. *European Radiology* 2003; **13**: 724–8. doi: https://doi.org/10.1007/s00330-002-1564-2
20. Harnish R, Prevrhal S, Alavi A, Zaidi H, Lang TF. The effect of metal artefact reduction on CT-based attenuation correction for PET imaging in the vicinity of metallic hip implants: a phantom study. *Ann Nuc Med* 2014; **28**: 540–50. doi: https://doi.org/10.1007/s12149-014-0844-7
21. van der Vos CS, Arens AIJ, Hamill JJ, Hofmann C, Panin VY, Meeuwis APW, et al. Metal artifact reduction of CT scans to improve PET/CT. *J Nucl Med* 2017; **58**: 1867–72. doi: https://doi.org/10.2967/jnumed.117.191171